Raman spectroscopy on hydrogenated graphene under high pressure

Teerachote Pakornchote[1,2,3], Zachary M. Geballe[3], Udomsilp Pinsook[1,2], Thiti Taychatanapat[4], Wutthikrai Busayaporn[5], Thiti Bovornratanaraks[1,2,*], Alexander F. Goncharov[3,6,7,*]

[1]Extreme Conditions Physics Research Laboratory, Physics of Energy Materials Research Unit, Department of Physics, Faculty of Science, Chulalongkorn University, Bangkok, 10330, Thailand

[2]Thailand Center of Excellence in Physics, Commission on Higher Education, 328 Si Ayutthaya Road, Bangkok, 10400, Thailand

[3]Geophysical Laboratory, Carnegie Institution of Washington, 5251 Broad Branch Road, Washington, DC 20015, USA

[4]Department of Physics, Faculty of Science, Chulalongkorn University, Bangkok, 10330, Thailand

[5]Synchrotron Light Research Institute (Public Organization), Nakhon Ratchasima 30000, Thailand

[6]Key Laboratory of Materials Physics and Center for Energy Matter in Extreme Environments, Institute of Solid State Physics, Chinese Academy of Sciences, Hefei, Anhui 230031, China

[7]University of Science and Technology of China, Hefei 230026, Anhui, People's Republic of China

---

Abstract

We applied laser-heating in diamond anvil cells (LHDAC) to synthesize a hydrogenated single-layer graphene (SLG) and to explore the pathway toward graphane (fully hydrogenated SLG). We employed Raman spectroscopy to investigate SLG on a Cu substrate that was compressed up to 8 GPa and 20 GPa with 2.2% and 4.6% compressive strain, respectively, followed by laser-heating. After laser-heating, G and 2D peaks exhibit a redshift, and then form a hysteresis loop during decompression. This phenomenon can be due to either of two mechanisms, or both; the formation of C-H chemical bonds in massive hydrogenated SLG, and a reduction of the frictional stress between SLG and Cu substrate causing a relaxation of SLG lattice toward its free-standing equilibrium structure. The correlation between G and $2D$ peaks also changes significantly after laser-heating at 8 GPa, resembling the correlation measured in hole-doping experiments. Finally, residual hydrogen remains bonded to the graphene layer after decompression to ambient pressure, and the amount of hydrogen increases as a function of pressure at which the sample was laser-heated.

Keywords: Hydrogenated graphene; Graphane; High pressure; Thermodynamic pathway; Raman spectroscopy;

---

corresponding authors, email: thiti.b@chula.ac.th, agoncharov@carnegiescinece.edu.

1. Introduction

Graphane, fully hydrogenated single-layer graphene (SLG), has a wide band gap [1], in contrast to pristine SLG, which has a zero band gap [2]. Graphane material is expected to possess a number of fascinating properties such as strong charge-transfer excitonic effects [3, 4] and a higher speed of spin-transport than GaAs, making it advantageous for spintronic applications [5]. To hydrogenate SLG, hydrogen plasma guns have been used to bombard hot hydrogen onto SLG surface [6, 7]. Hydrogen concentration in SLG increases with the bombarding time [6, 7]. The hydrogenation on SLG can be verified by several techniques such as scanning electron microscope (SEM), high-resolution electron energy loss spectroscopy (HREELS), and x-ray photoelectron spectroscopy (XPS) [7-12]. Band gap opening, has been confirmed by angle-resolved photoemission microscopy (APRES) [8, 11]. Thermal annealing can reverse hydrogenated SLG back to SLG [7, 13]. However, the use of the above technique results in partially hydrogenated SLG. Even though hydrogenated SLG is a potential candidate for many applications such as a reversible and tunable band gap [14, 15], field-effect transistor, and sensing applications [15, 16], the experimental methods to create fully hydrogenated graphane are still needed.

The two major thermodynamic factors that can be utilized to explore the synthesis pathway of graphane are temperature and pressure. Application of pressure often results in shifting the thermodynamic stability toward unusual chemical compositions (*e.g.*, Ref. [17]) that do not exist at ambient pressure, while one commonly needs high temperatures to start the transformation. Theoretical structure predictions in hydrocarbons at high pressures suggest that graphene with the CH composition can be thermodynamically stable above 7 GPa [18]. Several studies of graphene under high pressure show no chemical reactivity at room temperature with hydrogen and several other materials used as a pressure transmitting media (PTM); however, they are debating a possible charge transfer [19-22]. Smith *et al*. [23] studied hydrogenation on SLG by heating the SLG in H_2 at 200ºC under high pressure and monitoring the ratio of intensity of Raman band, $I(D)/I(G)$, where D and G stand for the defect and graphite modes, respectively. They concluded that the concentration of defects and bonded atoms of the recovered SLG, increases as a function of the applied pressure up to 5 GPa [23]. However, full hydrogenation has not been reached.

In this work, we study the hydrogenation on SLG using a laser to heat SLG on a Cu substrate under pressure up to 20 GPa to explore the hydrogenation pathway of SLG toward graphane. The results show that laser-heating of SLG beyond 1000 K at 8 and 20 GPa results in dramatic changes

of the vibrational properties recorded via *in situ* Raman spectroscopy and on the recovered sample. Below we present the following findings: 1) Raman spectra of the recovered samples reveal the amount of partial hydrogenation increasing with the pressure of laser-heating; 2) Laser-heating at 8 and 20 GPa results in dramatic softening of the G mode that can be understood as due to peeling off of SLG from the substrate by substantial hydrogenation; 3) A hysteresis loop of the Raman shift is observed on pressure release after laser-heating, and it can be explained by dehydrogenation of the sample and reattachment with the substrate; 4) The correlation between G and 2D peaks of SLG in H_2 PTM changes after laser-heating at 8 GPa, which suggests a hole-doping-like behavior of hydrogenated SLG.

2. Methodology and Experimental procedures

We use Raman spectroscopy to probe the effect of pressurization and laser-heating on SLG. The hydrogen concentration in SLG can be quantified by the ratio of intensities of Raman peaks, $I(D)/I(D')$ [24]. A theoretical study shows that this ratio can be used to assess the presence and amount of sp^3-bonding and vacancy defects [25], and that these two type of defects can be differentiated by $I(D)/I(D') \sim 7$ for vacancy-defect and ~ 13 for sp^3-defect [6]. The defective SLG can be classified by two stages according to the defect concentration (N_D): Stage 1 is when N_D is below approximately 7×10^{12} cm^{-2} and Stage 2 when it is higher [25]. In Stages 1 and 2, $I(D)$ becomes stronger and weaker with N_D, respectively, while $I(2D)$ decreases in both stages [25]. If the concentration of hydrogen (considered as the defects) is very high, then G and D' peaks merge and the Raman spectrum of hydrogenated SLG will be similar to that of amorphous carbon [26, 27].

In this work, we used SLG on a ~18 μm thick Cu substrate with from the Graphenea company and then cut it into pieces smaller than 70×70 μm^2 with a razor blade (Figure 1). A Re gasket was indented to 37-45 μm thickness and a ~190 μm diameter hole was drilled in the center of the indentation to form the high-pressure cavity. We used a symmetric diamond anvil cell (DAC) equipped with diamond anvils with the culet of ~300 μm diameter. Research grade hydrogen and helium gases (99.999% purity) were used as PTM and/or reactants in separate experiments. H_2 and He gas was loaded in the DAC at room temperature in a high-pressure vessel at 0.15-0.20 GPa. This is a standard procedure. A continuous 1065 nm laser with 10 nm linewidth FWHM was used for one-side laser-heating. Laser power was sequentially increased to reach the desired temperature of 1500 to 2000 K in a ~ 10 micron diameter heated area at the Cu-KCl interface. A CCD camera

with near IR sensitivity continuously monitored the heating process, and spectroradiometric temperature measurements were collected at discrete times. Raman spectra at high pressures [28] and of the recovered samples were recorded using a single-frequency solid-state laser with the wavelength of 488 nm and a single-stage grating spectrograph equipped with a CCD detector. The spectral resolution was 4 cm^{-1} when using a grating of 1500 grooves/mm. A custom-build confocal Raman microscope collected the signal in a back-scattering geometry using a Mitutoyo 20X, NA=0.4 objective lens; ultra-low frequency holographic solid-state notch filters allowed measurement of the spectra down to 10 cm^{-1}. Pressure was measured using ruby fluorescence scale [29].

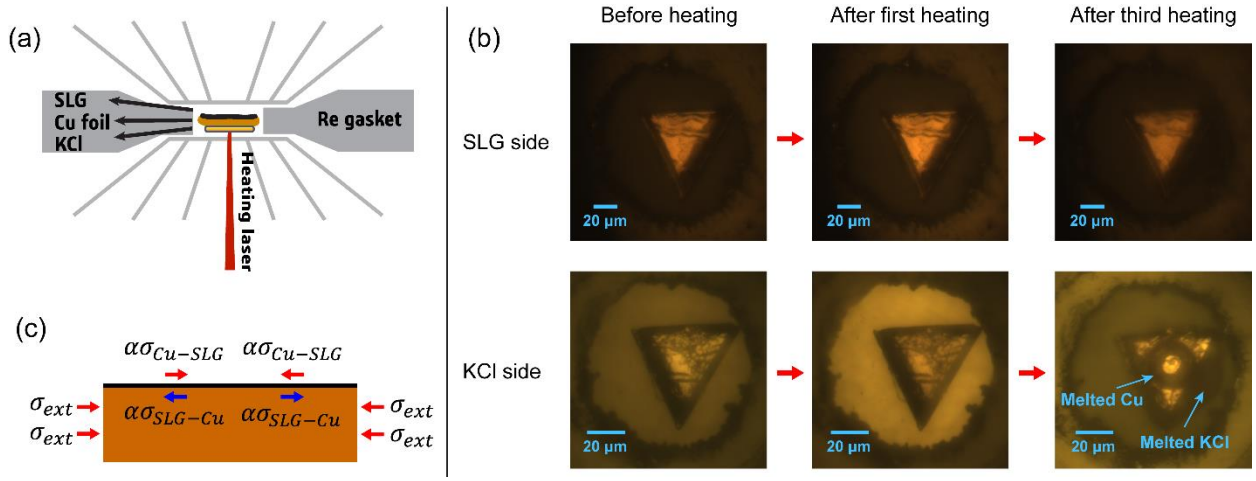

Figure 1. (a) Schematic of the DAC experiments. (b) Microphotographs of the sample of Run 1 taken in the reflected light. (c) A cartoon, which presents stresses acting on SLG and Cu substrate.

We performed three different experiments, which are named as follows. The first two experiments with SLG/Cu in hydrogen PTM laser-heated at 8 GPa and 20 GPa are Run 1 and Run 2, respectively. The control experiment with SLG/Cu in helium laser-heated at 8 GPa is Run 3. The thickness of Cu substrates in Run 1 and 3 was 18 μm, and it was polished down to approximately 10 μm in Run 2 to allow a relatively-thick layer of hydrogen between SLG and the diamond culet at 20 GPa (Figure 1). A ~3-5 μm thick KCl plate was positioned on one of the anvils as a thermal insulator for the Cu substrate placed on the top of it, while the other side with a graphene layer on it was facing H_2 or He. Laser-heating was applied for about 10 s on the graphene-free side of Cu substrate to avoid exposing graphene directly. In Run 1, the sample was heated 3 times, while in Run 2 and Run 3 the samples were heated 2 times. The laser power was sequentially

increased in these heating events to reach the desired temperature. The experiments were performed at the Geophysical Laboratory, Carnegie Institution for Science.

3. Results and discussion

3.1 Residual hydrogenation

After the samples of SLG on Cu substrate were laser-heated at 8 GPa and 20 GPa in H_2 PTM for Run 1 and Run 2, respectively, and at 8 GPa in He PTM for Run 3, the pressures were decreased to recover the sample at ambient pressure. Figure 2 shows comparative Raman spectra between the pristine and the recovered sample of Run 1, Run 2, and Run 3. For the samples in H2 PTM in Run 1 and Run 2, we observed the increase in the amount of defects (e.g., sp^3-defect, vacancy-defect) as evidenced by the increasing of $I(D)/I(G)$ [30, 31] . Our results are consistent with the other similar experiment from Smith et al [23].

In contrast, in Run 3 for SLG laser-heated in He PTM, the $I(D)/I(G)$ ratios of the pristine and the recovered sample are about the same, while D' peak cannot be resolved (see an inset in Figure 3). Thus, in the presence of He PTM, there is no enhancement of defects due to heating, in contrast to H_2 PTM, where defects on SLG were created even in the area far from the heated spot (see Figure 3).

The theoretical study using molecular dynamics simulation reveals that energy of ion bombardment onto SLG creating vacancy-defects is much higher than embedding adatoms [32, 33]. Since there is no defect enhancement after laser-heating of SLG in He PTM, the defects, which appear in Run 1 and Run 2, must originate from the hydrogenation.

Moreover, Machon *et al*. [34] discusses that if Ar is used as a PTM, solid Ar can cause shear stress on SLG and tear SLG into small pieces, which increases the density of edge-defects on SLG. A Raman study of edge-defects on graphene by Casiraghi *et al*. [35], shows that Raman spectra of SLG along the edge give $I(D)/I(G) < 1$. In contrast, the results in Runs 1 and 2 show $I(D)/I(G) > 1$ showing that the majority of D peak intensity must come from the defects other than the edge-defect and the edge-defect may contributes to D peak marginally. Consistently, Smith *et al*. [23] show that there is no enhancement of D peak in Raman spectrum SLG on Cu substrate when compressed in solid H_2 medium to 6 GPa, even without annealing. This suggests that different pressure media should be considered individually when treating the effects of the shear

stresses. It is likely that solid H_2 is much softer than solid Ar, causing the difference in Raman spectra.

Eckmann *et al*. [6] suggests that sp^3-defects and vacancy-defects can be identified by the ratio $I(D)/I(D')$ ~13 and ~7, respectively. For Run 1, $I(D)/I(D')$ are ~13 for spots nearby the heated spot, while $I(D)/I(D')$ are ~7 for spots far from the heated spot (see Figure 3). However, Figure S1 in SI shows that the spots far from the heated spot were heated to the temperature lower than the spots nearby the heated spot. As we have discussed in the previous paragraph, the defects of the spots, which have $I(D)/I(D')$ ~7 (see Figure 3), should not be vacancy-defect, but sp^3-defect. Therefore, Eckmann's condition [6] may fail in this case.

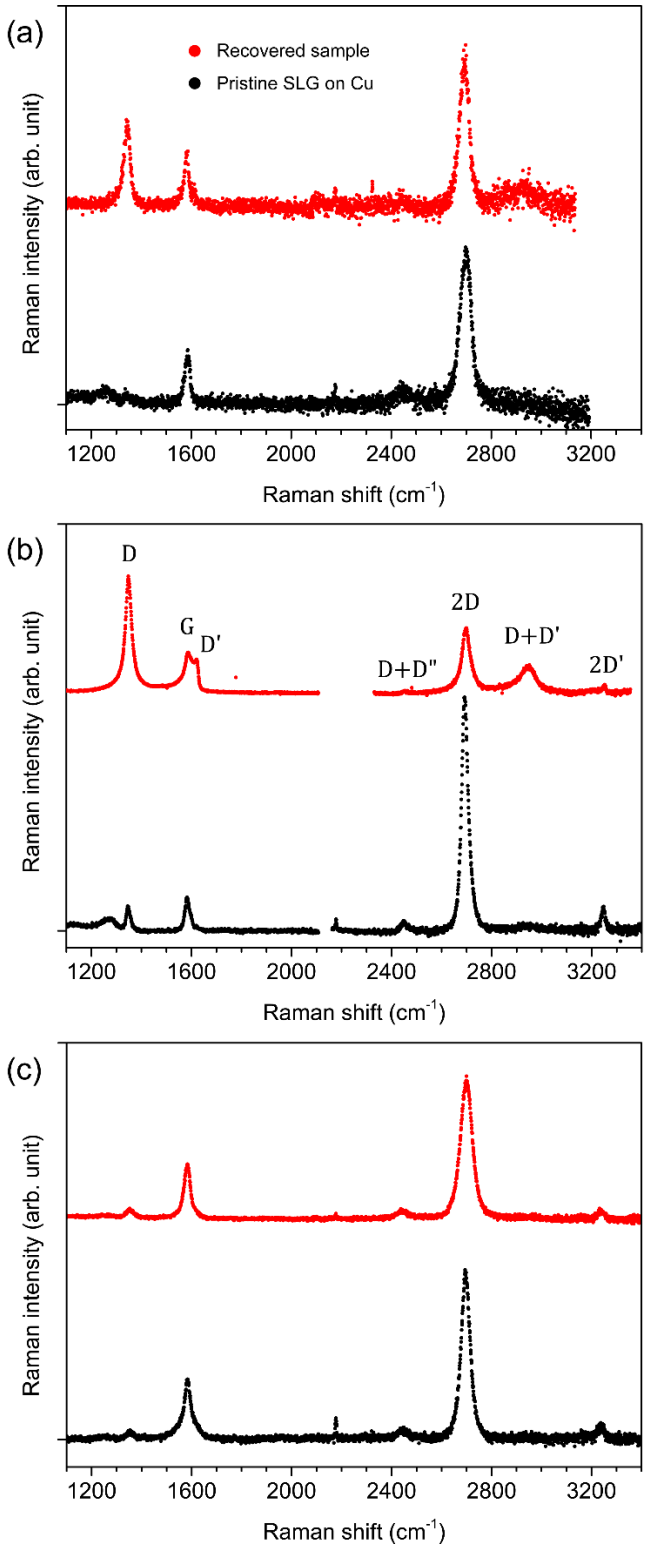

Figure 2. Raman spectra of the pristine SLG (black) and the recovered sample (red) from experiments; (a) Run 1 collected for 30s with 1 accumulation, (b) Run 2 collected for 60s with 5 accumulations, and (c) Run 3 collected for 60s with 1 accumulation. The signal-to-noise ratio is different for (a), (b), and (c) panels because of different accumulation times and because different laser powers were used. The spectra are

shifted vertically for clarity. All the spectra were measured with the samples residing on one of the diamond anvils, and the second anvil from the side of the Raman microscope was removed.

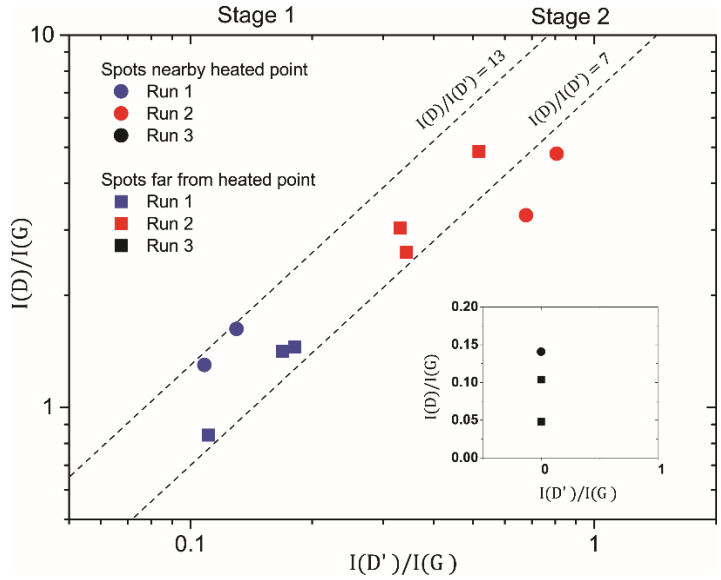

Figure 3. The intensity ratios of the Raman peaks for the recovered samples of Run 1 (blue), Run 2 (red), and Run 3 (black in the inset). The intensities are deduced from fitting with the Lorentzian lineshape for D and G modes, and the Breit-Wigner-Fano (BWF) lineshape for D' mode. Stage 1 (Stage 2) is for N_D which is less (more) than ~7x10^{12} cm^{-2}. This distinction arises from the nature of $I(D)$ which increases in Stage 1, but decreases in Stage 2 as N_D increases [25].

3.2 Pressurization, laser-heating, and a possible full hydrogenation at high pressure

In the previous section, the hydrogenation has been confirmed by the Raman spectra of the recovered samples. Herein, we will discuss the pressure treatment on SLG and hydrogenated SLG, and the possibility of full hydrogenation after laser-heating under high pressure. For Run 1, the Raman spectra were measured at 6 different positions around the sample repeatedly for each pressure point and temperature treatment. To extract the spectral positions/linewidths, the most prominent G and 2D Raman peaks were fitted to the Lorentzian line shape (see Figure S3 in SI).

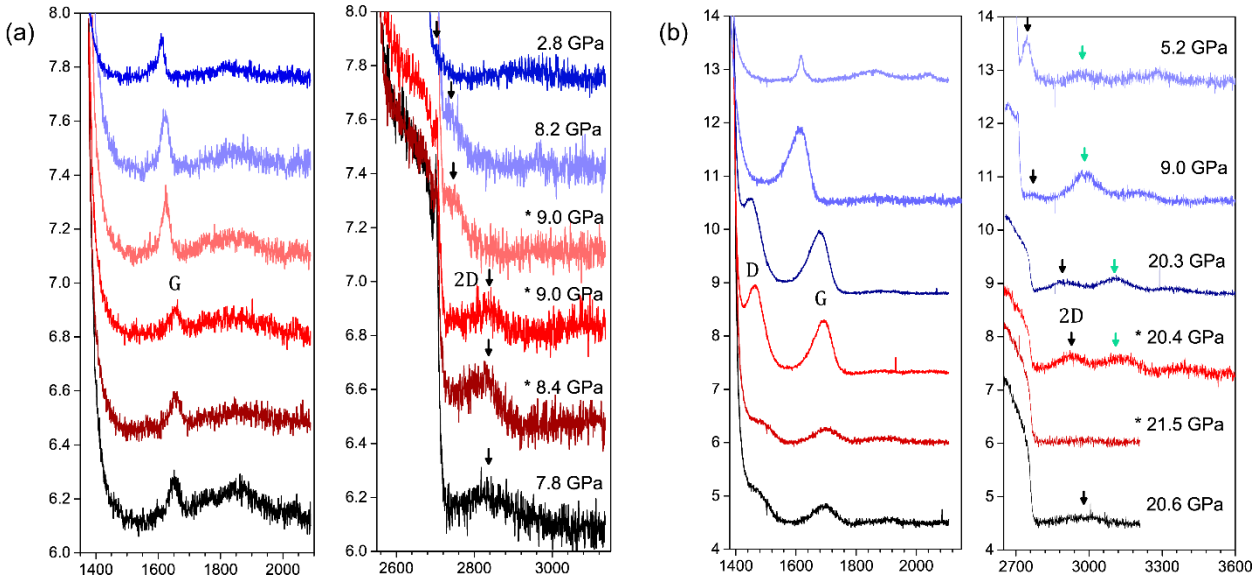

Figure 4. Raman spectra of graphene (intensity in arbitrary units versus Raman shift in wavenumbers) as the pressure evolves and sample is laser-heated in (a) Run 1 and (b) Run 2. Black curves- spectra before heating, various reddish curves -after the laser heating and blueish – on decompression. The asterisks (*) mark pressure values after the laser heating. Black and green down arrows show the position of 2D peak and the new peak, respectively. The scales on the y-axis are for comparing the intensities of Raman peak in different panels.

Figure 4 shows the evolution of the Raman spectra with pressure and heat treatment in Runs 1 and 2. The Raman shifts of G and 2D peaks (ω_G and ω_{2D}) measured at various sample positions are averaged and plotted in Figure 5 as a function of pressure. The error bars are the standard deviation of 6 data points taken at different positions for each pressure point. During compression, ω_G and ω_{2D} shift to higher frequencies as pressure increases (see Figure 5). The 2D peak decreases in intensity and becomes barely observed at high pressures. After the first two laser-heating events in Run 1, ω_G and ω_{2D} shift to lower frequencies noticeably, while the pressure remains almost the same within 1 GPa. During the third laser heating in Run 1, we noticed a strong visible light emission from the heated spot. An optical micrograph in Figure 1(d) shows that KCl and Cu around the heated spot melted, but the SLG side did not alter as observed visually. This suggests that the temperature on the heated Cu surface must have been greater than 2300 K (melting point of KBr is ~ 2300 K at 10 GPa [36], melting point of Cu is ~ 1600 K at 10 GPa [37]). However, the temperature on the SLG side must have been colder than the heated side because of the temperature gradients, which develop as the result of a steady heat transport from the hot spot to the surrounding materials (mainly axially via the diamond anvils). We evaluated the temperature at the SLG based

on the results of finite element calculations [38], which use the realistic geometric and thermochemical parameters (see Method S1 and Figure S1 in SI for details). We estimated the highest temperature at the SLG to be below 1200 K.

After laser-heating, the intensity of the redshifted G and 2D bands increases (Figure 4). In addition, in Run 2, the intensity of the D band increases dramatically, and an additional band appeared at nearly 3100 cm^{-1}. On the pressure release, the G and 2D bands follow different pressure dependencies than on compression forming a kind of hysteresis loops in Raman frequencies, which closes near 3 GPa. Please note that the 2D peak cannot be resolved in some sample areas during decompression, in which case the data were averaged over less than 6 data points. We interpret the hysteresis loops in G and 2D bands of Run 1 and Run 2 in terms of a slipping model in the next section.

To show that the population of sp^3-defects increases after the second laser heating in Run 2, N_D before and after laser heating are determined from $I(D)/I(G)$ using Eq. 8 from Ref. [31]. This equation gives two solutions of N_D which result in Stage 1 and Stage 2 (see Table S1 in SI). We justify that before laser heating the defective SLG should be in Stage 1 which has $N_D = 0.90\times10^{12}$ cm^{-2}, while after the second laser heating the defective and/or hydrogenated SLG should be in Stage 2 which has N_D and/or hydrogen concentration = 17.7×10^{12} cm^{-2} (see Table S1 in SI).

In the control Run 3 with He PTM to 9.4 GPa, there were slight drops of the Raman frequencies of the G and 2D peaks after heating (Figure 5). We find no substantial change in intensity of these peaks. The pressure dependencies of the frequencies do show a small hysteresis loop similarly to the experiments with H_2 (see Figure 5).

The Raman spectra modifications after laser-heating are intriguing as they suggest a possible massive hydrogenation of SLG at high pressure in accord with the theoretical predictions [18]. Indeed, one would expect the G band to soften in graphene [39] due to a distortion of the graphene flat atomic sheets. Run 2 shows the most prominent observations, where we observed an increase in intensity of all modes, which is consistent with the formation of sp^3 bonded carbon. Moreover, a new peak at 3100 cm^{-1} that appears after laser heating and remains on unloading down to ambient conditions could signal the formation of the C-H bonding. This new peak could be either $D + D'$ or C-H stretching modes which appear at the similar frequency at ambient pressure. For either assignment, the appearance of a new peak suggests the massive hydrogenation of SLG. For an

illustration, the highly sp^3-defected SLGs at ambient pressure also yield similar spectra where $2D$ and $D + D'$ peaks broaden and merge, and $I(2D)/I(D + D') \approx 1$ [24]. Similarly, after the second laser heating in Run 2, $I(2D)/I(G)$ and $I(\text{new peak})/I(G)$ are 0.30 and 0.26, respectively. Upon decompression, these ratios increase at pressure below 5.2 GPa (see Figure S5 in SI), but this increase is stronger for the 2D peak than for a new peak. This leaves a possibility that a new peak is the C-H mode.

To further investigate the new peak at ~3100 cm^{-1}, Raman spectra from a red laser (660 nm) were also collected in Run 2. Comparison of blue and red excited Raman spectra allow us to quantify dispersion, the variation of Raman peak position with energy of the excitation laser. Past studies have documented the dispersion of D and 2D peaks of graphene to be 50 and 100 cm^{-1}/eV, respectively [40]. After the second laser heating in Run 2 of the present study, the dispersions of D, 2D and the new peak are 30, 73 and 34 cm^{-1}/eV, respectively. Upon decompression, the dispersion of the new peak decreases to less than 30 cm^{-1}/eV (Figure S6 in SI). In contrast, the dispersions of 2D and $D + D'$ peaks of the recovered sample are much larger (227 and 217 cm^{-1}/eV), suggesting that the new peak is not the $D + D'$ peak at high pressure, but rather the C-H stretching mode.

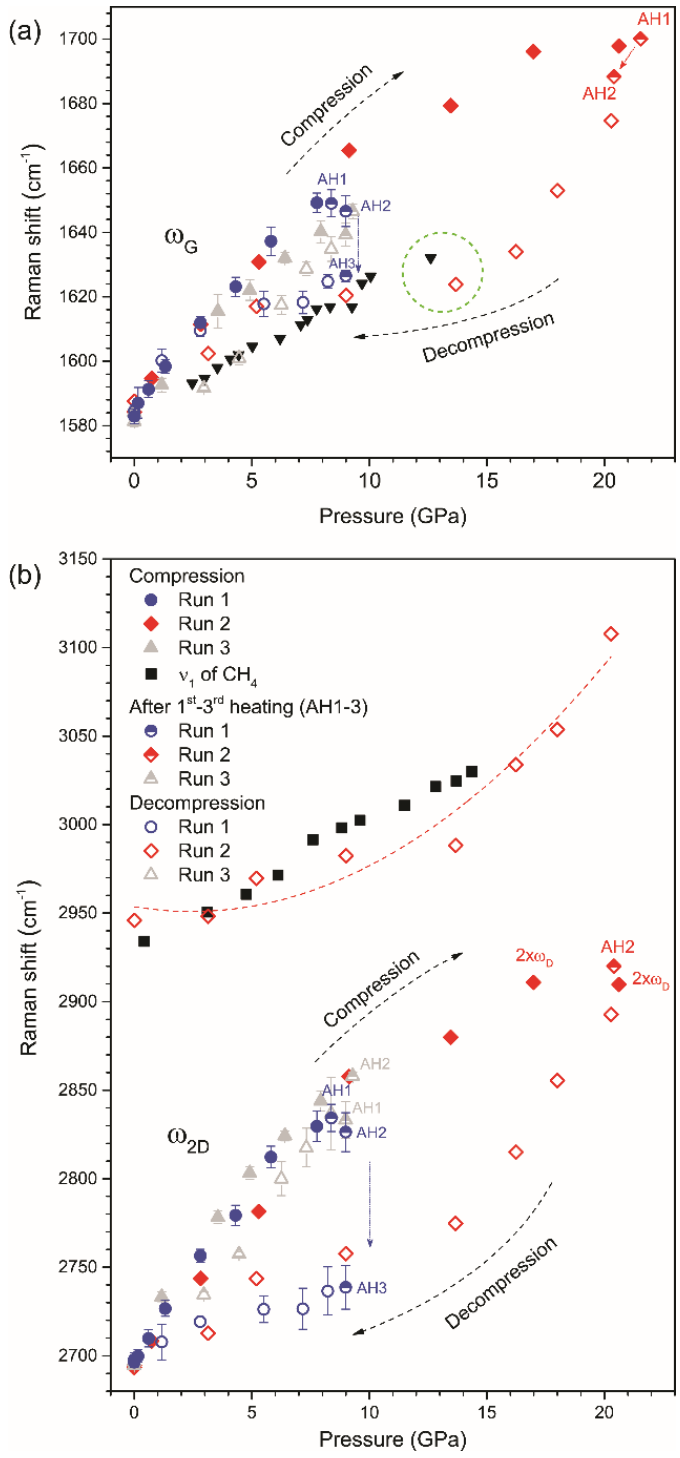

Figure 5. Raman shifts of peaks ω_G (a) and ω_{2D} (b) of SLG on Cu in Run 1 (blue circle), Run 2 (red diamond), and Run 3 (grey triangle) as a function of pressure during compression (filled symbols), after laser-heating (semi-filled symbols), and during decompression (open symbols). Red-dashed line in (b) is a guide to the eye of a new peak (see text) fitted with a quadratic equation. Dark down-triangles are the data for SLG on diamond from Ref. [41]. Black filled squares are the data for the ν_1 C-H stretching mode of methane obtained in this work in a separate experiment. The points labeled by $2 \times \omega_D$ is the doubled frequency of the D peak (as the 2D peak could not be measured).

3.3 Total stress and frictional stress on SLG

Figure 5 shows that ω_G and ω_{2D} shift to lower frequency drastically after laser-heating and their pressure dependencies reveal a hysteresis loop upon decompression. Similar phenomena have been noticed in previous works (albeit without laser-heating), where qualitatively, the more compressible substrate induces a compressive traction on the SLG, causing extra stress and hence an increase in ω_G and ω_{2D} [41, 42]. After laser-heating, SLG slips on the substrate, reducing these tractions, resulting in redshifted ω_G and ω_{2D}. This model provides a simple explanation to a variety of the pressure gradients observed for G band as well for its abrupt frequency drops under pressure.

Because ω_G is an intrinsic vibrational frequency of SLG subjugated to applied strain, the strain on SLG can be calculated without considering the substrate, [42, 43]

$$\varepsilon(\omega_G) = -\beta(\omega_G - 1583), \quad (1)$$

where β, equals to 3.99×10^{-4} cm, is a constant calculated from the Poisson's ratio, 0.167 [43], the Grüneisen parameter of phonon G mode, 1.90 (see Method S2 in SI for details), and 1583 cm^{-1} which is ω_G for SLG on Cu substrate averaged from data in Run 1. Therefore, the highest strains of SLGs before laser-heating are 2.6% for Run 1 at 8 GPa, 4.6% for Run 2 at 20 GPa, and 2.3% for Run 3 at 8 GPa.

To account for the effect of the substrate on SLG we use a model, which accounts for friction between SLG and the Cu substrate. We assume that SLG is held by Cu substrate by a frictional stress ($\alpha_i \sigma_{Cu-SLG}$) causing an area of SLG to expand or shrink together with its substrate. Under pressure, SLG is affected by the external stress (σ_{ext}) and the frictional stress between SLG and Cu substrate (see a cartoon in Figure 1(c)). Thus, the total stress on SLG is

$$\sigma_{SLG} = \sigma_{ext} + \alpha_i \sigma_{Cu-SLG}, \quad (2)$$

where α_i is a coefficient of frictional stress between Cu surface and SLG at pressure point i, and σ_{Cu-SLG} is a frictional stress supporting the equal deformation of the SLG area and Cu contact area (see Figure S9 in SI). It is worth noting that Francisco-López *et al*. [44] proposes that the 2-dimentional materials such SLG are not affected by the external stress, however this hypothesis requires separate experimental confirmation. Here, we consider that the total stress, causing a compressive strain on SLG, shrinks the area of SLG per unit cell by,

$$-2\beta\Delta\omega_G + \beta^2(\Delta\omega_G)^2 = \lambda_{SLG}\sigma_{SLG}, \quad (3)$$

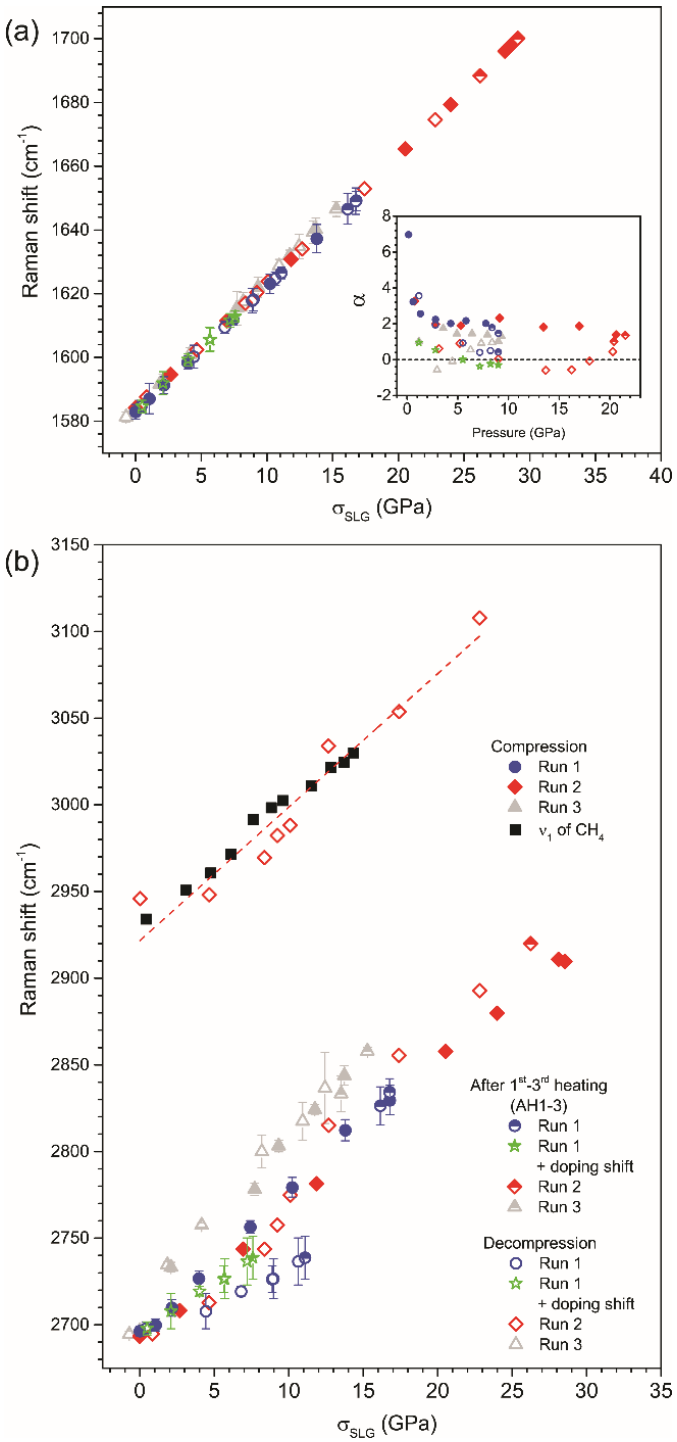

Figure 6. (a) ω_G and (b) ω_{2D} of SLG on Cu as a function of total in-plane stress acting on SLG. An inset in (a) shows the friction coefficient as a function of pressure deduced from our Raman frequency data. Red-dashed line in (b) is a guide to the eye of a new peak (see text) fitted with a linear equation. All symbols are the same representation as in Figure 5. Green stars are data corrected by $\Delta\omega_d$ (see text).

where the left hand side is the area of SLG per unit cell written as a function of ω_G (see Method S2 in SI for a derivation), and λ_{SLG} is a fitting parameter for SLG. Bousige *et al*. [41] shows that SLG on diamond substrate has $\partial\omega_G/\partial P$ similar to graphite. Graphite is stacked of layers of graphene, where every layer is weakly connected to, so they contract independently under high pressure. Thus, the frictional stress between layers is assumed to be very small and can be neglected, yielding $\sigma_{SLG} \approx \sigma_{ext} = P$, yielding the Eq. 3 in the form

$$-2\beta\Delta\omega_G + \beta^2(\Delta\omega_G)^2 = \lambda_{SLG}P, \tag{4}$$

where P is a pressure. Hence, we use Eq. (4) to obtain λ_{SLG} by fitting $\Delta\omega_G$, which is data of SLG on diamond substrate from Ref. [41], with P.

In the present work, the Raman frequencies ω_G and ω_{2D} as a function of σ_{SLG} are shown in Figure 6, where σ_{SLG} is calculated using Eq. (3) where $\lambda_{SLG} = -0.0031$ GPa^{-1} (see Table S2 and Figure S10 in SI). Figure 6(a) shows that ω_G is linearized with σ_{SLG}, and the hysteresis loops for ω_{2D} (see Figure 6(b)) are depleted in all runs except that of ω_{2D} in Run 1. Since the mechanical properties of partially hydrogenated SLG are similar to those of pristine SLG [45, 46], we assumed that the Grüneisen parameter of the phonon G mode and the Poisson's ratio of partially hydrogenated SLG are the same c I; as those of the pristine SLG. Figure 6 suggests that the major origin of the hysteresis loop must come from the alteration of the frictional stress between Cu substrate and SLG.

The inset in Figure 6(a) presents the coefficient of frictional stress, calculated by

$$\alpha_i = \frac{1}{\eta_i}\left[\frac{(\lambda_{Cu_1} - \eta_i\lambda_{SLG})\sigma_{ext} + \lambda_{Cu_2}\sigma_{ext}^2}{(\lambda_{Cu_1} - \lambda_{SLG})\sigma_{ext} + \lambda_{Cu_2}\sigma_{ext}^2}\right], \tag{5}$$

where λ_{Cu_1} and λ_{Cu_2} are fitting parameters of Cu area versus external stress extracted from Ref. [47] (see Method S2 in SI for a derivation), and η_i is defined as

$$\left(\frac{V_{Cu}(P)}{V_{Cu}(0)}\right)^{2/3} - 1 = \eta_i(-2\beta\Delta\omega_G + \beta^2(\Delta\omega_G)^2), \tag{6}$$

where $V_{Cu}(P)$ is a volume of Cu per unit cell as a function of pressure. After the third laser-heating in Run 1, α_i drops from 7.0 at 0.2 GPa to 2.2 at 2.8 GPa, and significantly drops to 0.4 (see an inset in Figure 6(a)) indicating that SLG is almost detached from the Cu substrate completely. The similar results hold for Run 2 and Run 3 as well. Hence, laser-heating of the

sample at a certain temperature loosens a contact between SLG and Cu substrate. The detachment may occur because the Cu lattice expands, but SLG lattice shrinks at high temperature [48-50].

3.4 Correlation between ω_G and ω_{2D}

Here we discuss the correlation between ω_G and ω_{2D}, and why it changes after laser heating. On compression, ω_G is linearly related with ω_{2D}, and the $\partial\omega_{2D}/\partial\omega_G$ in Runs 1, 2 and 3 are 2.2, 2.0 and 2.5 (see Figure 7), respectively, which is in agreement with other experiments [42, 51, 52]. The dashed lines in Figure 7, extracted from Ref. [52], represent the correlation between ω_G and ω_{2D} of SLG when it is affected by purely strain (e_T line), purely hole-doped (e_H line), and concurrently strain and hole-doped [52]. In Run 1, the correlation between ω_G and ω_{2D} of the sample after third laser-heating shown in Figure 7 significantly changes from on the e_T line to near the e_H line. This indicates that the Raman spectrum of the quenched sample behaves as if it were hole-doped. Noting that Ref. [52] shows the line of hole-doping up to $15\text{x}10^{12}$ cm^{-12}, we extrapolate the hole concentration lines up to $30\text{x}10^{12}$ cm^{-2} to cover our data by assuming that the line of hole concentration constantly changes with strain.

On the one hand, it may be unreliable to justify that the hydrogenated SLG is chemically hole-doped, since the $\partial\omega_{2D}/\partial\omega_G$ of strained SLG is not restricted to be 2.2 as we extracted from Ref. [52]. For example, the correlation between ω_G and ω_{2D} of Runs 2 and 3 are under and above, respectively, the e_T line (see Figure 7) in compression. On the other hand, to the best of our knowledge there is no other explanations about the change of the correlation between ω_G and ω_{2D} of SLG. Therefore, we include the charge-doping effect, which shifts the ω_G as a function of charge concentration [53, 54], into the analysis. The Eq. 1, hence, is reformulated to

$$\varepsilon = -\beta(\omega_G - \Delta\omega_d(n) - 1583), \quad (7)$$

where $\Delta\omega_d(n)$ is added to correct a frequency shift as a function of charge-doping, n. The hole-doping concentration of each data point is extracted from the plot in Figure 7, and $\Delta\omega_d(n)$ can be calculated using Eq. 6 in Ref. [54] at 300 K (see Figure S13 in SI). The application of the doping correction via Eq. 7 makes the total stress on the sample and the hysteresis loop of ω_{2D} of Run 1 smaller (see green star symbols in Figures 6a,b). In the calculation, Fermi velocity (v_F) is considered as an invariant parameter, but v_F should depend on applied strain [55], and charge-doping [56] that would be a reason of the persistent discrepancy between compression and

decompression data of ω_{2D} of Run 1 (see Figure 6(b)). However, to firmly support this conclusion more experiments need to be performed.

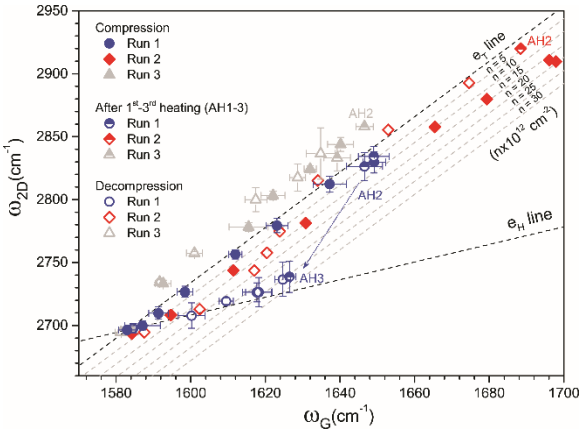

Figure 7. The correlations between ω_G and ω_{2D} of the sample during pressure treatment. All symbols are the same as in Figure 5. The e_T and e_H lines (black dashed line) are the guiding lines marking SLG affected by strain and hole-doping, respectively. The grey dashed lines labeled by n = 5, …, 30 are the guiding lines marking SLG affected concurrently by strain and hole-doping. The slope of the e_T line is 2.2, and the slope of the e_H line is 0.7.

3.5 Massive hydrogenation or detachment from the substrate?

We have discussed the possibilities of massive hydrogenation and the alteration of frictional stress between Cu substrate and SLG that cause the hysteresis loops of ω_G and ω_{2D}. The slipping model seems to explain the results well by diminishing of the hysteresis loops of ω_G and ω_{2D} shown in Figure 6. However, a downside of the slipping model is that we use all the parameters from the pristine SLG for hydrogenated SLG.

A theoretical study shows that the C-C bond length of graphane is longer than that of SLG [39], and the calculated optical phonon frequency at Γ-point of graphane is 1310 cm^{-1} at 0 GPa and 1350 cm^{-1} at 10 GPa [39], indicating the cause of the softening of ω_G of SLG after laser heating. Even though graphane is not thermodynamically stable at ambient pressure [18], it becomes stable under pressure and it could be metastable down to almost ambient pressure as evidenced by the presence of 3100 cm^{-1} band on unloading in Run 2 (Figure 4(b)), which can be interpreted as the C-H stretching mode. The theoretical study using Monte Carlo simulation demonstrated that H atoms prefer to form dangling bonds with C atoms on both sides of SLG and stay in close proximity to each other [57]. H_2 could penetrate through the gap between Cu and SLG to hydrogenate SLG from the substrate side during laser heating, causing a massive hydrogenation to occur. For

example, a dashed circle in Figure 5(a) marks that ω_G of hydrogenated SLG on Cu substrate is lower than ω_G of SLG on diamond substrate at similar pressure. For this case, the massive hydrogenation, causing the average C-C bond length of hydrogenated SLG longer than SLG, is a better explanation. Therefore, the massive hydrogenation and the detachment together can cause a tremendous redshift of ω_G.

Moreover, in decompression, ω_G of hydrogenated SLG on Cu substrate is higher than ω_G of SLG on diamond substrate at ~5 GPa (see open trapezoid and down-triangle symbols at 5 GPa in Figure 5(a)). The shortening of C-C bond length as pressure decreases can be explained by dehydrogenation from massively to partially hydrogenated SLG.

Yet another alternative explanation of the drop in ω_G after laser heating could be a structural transition in SLG similar to that reported in graphite [58, 59] or graphdiyne [60]. Evidently, the linewidth of the G band at 4.6% of compressive strain is six-fold larger than that of pristine SLG (see Figure S8(a) in SI), similar to phase transformation in graphite [61, 62]. The broadened G peak may come from the convolution of several peaks appearing because of the existence of several C-C bond lengths in the structure as well as a large disorder or even amorphization [63] originating from the corrugation of SLG on Cu substrate. However, to discuss this phenomenon qualitatively, more data is needed which is beyond the scope of the present work.

4. Conclusion

We performed laser heating of SLG deposited on Cu substrate in hydrogen medium in DAC at high pressure to explore its possible hydrogenation. The *in situ* was compressed to 8 and 20 GPa which the compressive strains (the total in-plane stresses) of SLG on Cu substrate were 2.6% and 4.6% (16.6 and 29 GPa), respectively, where the total in-plane stress is a summation of stress from *in situ* acting on the sample and frictional stress between SLG and Cu substrate. After laser treatment, the Raman frequencies of the G and 2D modes decreases, which is partially explained by the model where SLG detaches from Cu substrate. However, the appearance of additional Raman bands and some amount of softening could be tentatively assigned to a massive hydrogenation. However, more works need to be done to demonstrate synthesis of graphane at these conditions. The correlation between ω_G and ω_{2D} shows that hydrogenated SLG is likely to behave as being hole-doped under high pressure. The recovered SLG samples after pressure-

temperature treatments retain an amount of hydrogenation increasing with the pressure at which they were treated, presenting a possible pathway toward the graphene synthesis.

Acknowledgment

T.P. is very grateful to the Royal Golden Jubilee (RGJ) Ph.D. program (PHD/0197/2559) for the grant and financial support. This work was partially supported by Super SCI-IV research grant, Faculty of Science and Ratchadaphiseksomphot Endowment Fund of Chulalongkorn University, Grant for Research. This work was also supported by the NSF EAR-1763287, the Army Research Office, the Deep Carbon Observatory, and the Carnegie Institution of Washington. T. T. acknowledges support from Research Grant for New Scholar Ratchadaphiseksomphot Endowment Fund Chulalongkorn University (Grant No. RGN_2559_047_15_23).

References

[1] J.O. Sofo, A.S. Chaudhari, G.D. Barber, Graphane: A two-dimensional hydrocarbon, Phys Rev B 75(15) (2007).
[2] B. Partoens, F.M. Peeters, From graphene to graphite: Electronic structure around the K point, Phys Rev B 74(7) (2006).
[3] W. Wei, T. Jacob, Strong charge-transfer excitonic effects in C4H-type hydrogenated graphene, Phys Rev B 86(16) (2012).
[4] P. Cudazzo, C. Attaccalite, I.V. Tokatly, A. Rubio, Strong Charge-Transfer Excitonic Effects and the Bose-Einstein Exciton Condensate in Graphane, Phys Rev Lett 104(22) (2010).
[5] R. Zapata-Pena, B.S. Mendoza, A.I. Shkrebtii, Pure spin current injection in hydrogenated graphene structures, Phys Rev B 96(19) (2017).
[6] A. Eckmann, A. Felten, A. Mishchenko, L. Britnell, R. Krupke, K.S. Novoselov, C. Casiraghi, Probing the Nature of Defects in Graphene by Raman Spectroscopy, Nano Lett 12(8) (2012) 3925-3930.
[7] Z.Q. Luo, T. Yu, K.J. Kim, Z.H. Ni, Y.M. You, S. Lim, Z.X. Shen, S.Z. Wang, J.Y. Lin, Thickness-Dependent Reversible Hydrogenation of Graphene Layers, Acs Nano 3(7) (2009) 1781-1788.
[8] R. Balog, B. Jorgensen, L. Nilsson, M. Andersen, E. Rienks, M. Bianchi, M. Fanetti, E. Laegsgaard, A. Baraldi, S. Lizzit, Z. Sljivancanin, F. Besenbacher, B. Hammer, T.G. Pedersen, P. Hofmann, L. Hornekaer, Bandgap opening in graphene induced by patterned hydrogen adsorption, Nat Mater 9(4) (2010) 315-319.
[9] L. Kyhl, R. Balog, T. Angot, L. Hornekaer, R. Bisson, Hydrogenated graphene on Ir(111): A high-resolution electron energy loss spectroscopy study of the vibrational spectrum, Phys Rev B 93(11) (2016).
[10] R. Balog, M. Andersen, B. Jorgensen, Z. Sljivancanin, B. Hammer, A. Baraldi, R. Larciprete, P. Hofmann, L. Hornekaer, S. Lizzit, Controlling Hydrogenation of Graphene on Ir(111), Acs Nano 7(5) (2013) 3823-3832.
[11] J.H. Jorgensen, A.G. Cabo, R. Balog, L. Kyhl, M.N. Groves, A.M. Cassidy, A. Bruix, M. Bianchi, M. Dendzik, M.A. Arman, L. Lammich, J.I. Pascual, J. Knudsen, B. Hammer, P. Hofmann, L. Hornekaer, Symmetry-Driven Band Gap Engineering in Hydrogen Functionalized Graphene, Acs Nano 10(12) (2016) 10798-10807.
[12] L. Kyhl, R. Bisson, R. Balog, M.N. Groves, E.L. Kolsbjerg, A.M. Cassidy, J.H. Jorgensen, S. Halkjaer, J.A. Miwa, A.G. Cabo, T. Angot, P. Hofmann, M.A. Arman, S. Urpelainen, P. Lacovig, L. Bignardi, H. Bluhm, J. Knudsen, B. Hammer, L. Hornekaer, Exciting H-2 Molecules for Graphene Functionalization, Acs Nano 12(1) (2018) 513-520.
[13] S. Ryu, M.Y. Han, J. Maultzsch, T.F. Heinz, P. Kim, M.L. Steigerwald, L.E. Brus, Reversible Basal Plane Hydrogenation of Graphene, Nano Lett 8(12) (2008) 4597-4602.
[14] D. Haberer, D.V. Vyalikh, S. Taioli, B. Dora, M. Farjam, J. Fink, D. Marchenko, T. Pichler, K. Ziegler, S. Simonucci, M.S. Dresselhaus, M. Knupfer, B. Buchner, A. Gruneis, Tunable Band Gap in Hydrogenated Quasi-Free-standing Graphene, Nano Lett 10(9) (2010) 3360-3366.

[15] J. Son, S. Lee, S.J. Kim, B.C. Park, H.K. Lee, S. Kim, J.H. Kim, B.H. Hong, J. Hong, Hydrogenated monolayer graphene with reversible and tunable wide band gap and its field-effect transistor, Nat Commun 7 (2016).
[16] L. Jiang, W.Y. Fu, Y.Y. Birdja, M.T.M. Koper, G.F. Schneider, Quantum and electrochemical interplays in hydrogenated graphene, Nat Commun 9 (2018).
[17] W.W. Zhang, A.R. Oganov, A.F. Goncharov, Q. Zhu, S.E. Boulfelfel, A.O. Lyakhov, E. Stavrou, M. Somayazulu, V.B. Prakapenka, Z. Konopkova, Unexpected Stable Stoichiometries of Sodium Chlorides, Science 342(6165) (2013) 1502-1505.
[18] A.S. Naumova, S.V. Lepeshkin, A.R. Oganov, Hydrocarbons under pressure: phase diagrams and surprising new compounds in the C-H system, arXiv e-prints, 2019.
[19] K. Filintoglou, N. Papadopoulos, J. Arvanitidis, D. Christofilos, O. Frank, M. Kalbac, J. Parthenios, G. Kalosakas, C. Galiotis, K. Papagelis, Raman spectroscopy of graphene at high pressure: Effects of the substrate and the pressure transmitting media, Phys Rev B 88(4) (2013).
[20] J.E. Proctor, E. Gregoryanz, K.S. Novoselov, M. Lotya, J.N. Coleman, M.P. Halsall, High-pressure Raman spectroscopy of graphene, Phys Rev B 80(7) (2009).
[21] K. Filintoglou, D. Kokkinos, D. Christofilos, J. Arvanitidis, O. Frank, M. Kalbac, K. Papagelis, S. Ves, G.A. Kourouklis, High pressure Raman studies of single- and bi-layer graphene on copper, J Phys Conf Ser 950 (2017).
[22] J. Nicolle, D. Machon, P. Poncharal, O. Pierre-Louis, A. San-Miguel, Pressure-Mediated Doping in Graphene, Nano Lett 11(9) (2011) 3564-3568.
[23] D. Smith, R.T. Howie, I.F. Crowe, C.L. Simionescu, C. Muryn, V. Vishnyakov, K.S. Novoselov, Y.J. Kim, M.P. Halsall, E. Gregoryanz, J.E. Proctor, Hydrogenation of Graphene by Reaction at High Pressure and High Temperature, Acs Nano 9(8) (2015) 8279-8283.
[24] A. Eckmann, A. Felten, I. Verzhbitskiy, R. Davey, C. Casiraghi, Raman study on defective graphene: Effect of the excitation energy, type, and amount of defects, Phys Rev B 88(3) (2013).
[25] P. Venezuela, M. Lazzeri, F. Mauri, Theory of double-resonant Raman spectra in graphene: Intensity and line shape of defect-induced and two-phonon bands, Phys Rev B 84(3) (2011).
[26] A.C. Ferrari, J. Robertson, Resonant Raman spectroscopy of disordered, amorphous, and diamondlike carbon, Phys Rev B 64(7) (2001).
[27] C. Casiraghi, A.C. Ferrari, J. Robertson, Raman spectroscopy of hydrogenated amorphous carbons, Phys Rev B 72(8) (2005).
[28] A.F. Goncharov, Raman Spectroscopy at High Pressures, Int. J. Spectrosc.2011.
[29] H.K. Mao, J. Xu, P.M. Bell, Calibration of the Ruby Pressure Gauge to 800-Kbar under Quasi-Hydrostatic Conditions, J Geophys Res-Solid 91(B5) (1986) 4673-4676.
[30] L.G. Cancado, A. Jorio, E.H.M. Ferreira, F. Stavale, C.A. Achete, R.B. Capaz, M.V.O. Moutinho, A. Lombardo, T.S. Kulmala, A.C. Ferrari, Quantifying Defects in Graphene via Raman Spectroscopy at Different Excitation Energies, Nano Lett 11(8) (2011) 3190-3196.
[31] M.M. Lucchese, F. Stavale, E.H.M. Ferreira, C. Vilani, M.V.O. Moutinho, R.B. Capaz, C.A. Achete, A. Jorio, Quantifying ion-induced defects and Raman relaxation length in graphene, Carbon 48(5) (2010) 1592-1597.
[32] X. Wu, H.Y. Zhao, M.L. Zhong, H. Murakawa, M. Tsukamoto, Molecular dynamics simulation of graphene sheets joining under ion beam irradiation, Carbon 66 (2014) 31-38.
[33] X.M. Qin, T.H. Gao, W.J. Yan, X.T. Guo, Q. Xie, Molecular dynamics simulation of graphene bombardment with Si ion, J Mol Struct 1061 (2014) 19-25.
[34] D. Machon, C. Bousige, R. Alencar, A. Torres-Dias, F. Balima, J. Nicolle, G.D. Pinheiro, A.G.S. Souza, A. San-Miguel, Raman scattering studies of graphene under high pressure, J Raman Spectrosc 49(1) (2018) 121-129.
[35] C. Casiraghi, A. Hartschuh, H. Qian, S. Piscanec, C. Georgi, A. Fasoli, K.S. Novoselov, D.M. Basko, A.C. Ferrari, Raman Spectroscopy of Graphene Edges, Nano Lett 9(4) (2009) 1433-1441.
[36] R. Boehler, M. Ross, D.B. Boercker, High-pressure melting curves of alkali halides, Phys Rev B 53(2) (1996) 556-563.
[37] S. Japel, B. Schwager, R. Boehler, M. Ross, Melting of copper and nickel at high pressure: The role of d electrons, Phys Rev Lett 95(16) (2005).
[38] J.A. Montoya, A.F. Goncharov, Finite element calculations of the time dependent thermal fluxes in the laser-heated diamond anvil cell, J Appl Phys 111(11) (2012).
[39] X.D. Wen, L. Hand, V. Labet, T. Yang, R. Hoffmann, N.W. Ashcroft, A.R. Oganov, A.O. Lyakhov, Graphane sheets and crystals under pressure, P Natl Acad Sci USA 108(17) (2011) 6833-6837.
[40] A.C. Ferrari, D.M. Basko, Raman spectroscopy as a versatile tool for studying the properties of graphene, Nat Nanotechnol 8(4) (2013) 235-246.

[41] C. Bousige, F. Balima, D. Machon, G.S. Pinheiro, A. Torres-Dias, J. Nicolle, D. Kalita, N. Bendiab, L. Marty, V. Bouchiat, G. Montagnac, A.G. Souza, P. Poncharal, A. San-Miguel, Biaxial Strain Transfer in Supported Graphene, Nano Lett 17(1) (2017) 21-27.
[42] T.M.G. Mohiuddin, A. Lombardo, R.R. Nair, A. Bonetti, G. Savini, R. Jalil, N. Bonini, D.M. Basko, C. Galiotis, N. Marzari, K.S. Novoselov, A.K. Geim, A.C. Ferrari, Uniaxial strain in graphene by Raman spectroscopy: G peak splitting, Gruneisen parameters, and sample orientation, Phys Rev B 79(20) (2009).
[43] Y.C. Cheng, Z.Y. Zhu, G.S. Huang, U. Schwingenschlogl, Gruneisen parameter of the G mode of strained monolayer graphene, Phys Rev B 83(11) (2011).
[44] A. Francisco-Lopez, B. Han, D. Lagarde, X. Marie, B. Urbaszek, C. Robert, A.R. Goni, On the impact of the stress situation on the optical properties of WSe2 monolayers under high pressure, Pap Phys-La Plata 11 (2019).
[45] E. Cadelano, P.L. Palla, S. Giordano, L. Colombo, Elastic properties of hydrogenated graphene, Phys Rev B 82(23) (2010).
[46] A. Weerasinghe, A.R. Muniz, A. Ramasubramaniam, D. Maroudas, Mechanical properties of hydrogenated electron-irradiated graphene, J Appl Phys 120(12) (2016).
[47] L. Liu, M. Liu, H. Verbeek, C.H. Hoffner, G. Will, Comparative compressibility of Cu, Ag and Au, Journal of Physics and Chemistry of Solids 51(5) (1990) 435-438.
[48] D. Yoon, Y.W. Son, H. Cheong, Negative Thermal Expansion Coefficient of Graphene Measured by Raman Spectroscopy, Nano Lett 11(8) (2011) 3227-3231.
[49] W.Z. Bao, F. Miao, Z. Chen, H. Zhang, W.Y. Jang, C. Dames, C.N. Lau, Controlled ripple texturing of suspended graphene and ultrathin graphite membranes, Nat Nanotechnol 4(9) (2009) 562-566.
[50] N. Mounet, N. Marzari, First-principles determination of the structural, vibrational and thermodynamic properties of diamond, graphite, and derivatives, Phys Rev B 71(20) (2005).
[51] J. Zabel, R.R. Nair, A. Ott, T. Georgiou, A.K. Geim, K.S. Novoselov, C. Casiraghi, Raman Spectroscopy of Graphene and Bilayer under Biaxial Strain: Bubbles and Balloons, Nano Lett 12(2) (2012) 617-621.
[52] J.E. Lee, G. Ahn, J. Shim, Y.S. Lee, S. Ryu, Optical separation of mechanical strain from charge doping in graphene, Nat Commun 3 (2012).
[53] M. Lazzeri, A.M. Saitta, F. Mauri, Breakdown of the adiabatic approximation in a doped graphene monolayer and in metallic carbon nanotubes, Phys Status Solidi B 244(11) (2007) 4118-4123.
[54] S. Pisana, M. Lazzeri, C. Casiraghi, K.S. Novoselov, A.K. Geim, A.C. Ferrari, F. Mauri, Breakdown of the adiabatic Born-Oppenheimer approximation in graphene, Nat Mater 6(3) (2007) 198-201.
[55] V.M. Pereira, A.H. Castro Neto, N.M.R. Peres, Tight-binding approach to uniaxial strain in graphene, Phys Rev B 80(4) (2009).
[56] D.C. Elias, R.V. Gorbachev, A.S. Mayorov, S.V. Morozov, A.A. Zhukov, P. Blake, L.A. Ponomarenko, I.V. Grigorieva, K.S. Novoselov, F. Guinea, A.K. Geim, Dirac cones reshaped by interaction effects in suspended graphene, Nat Phys 7(9) (2011) 701-704.
[57] H.J. Xiang, E.J. Kan, S.H. Wei, M.H. Whangbo, J.L. Yang, "Narrow" Graphene Nanoribbons Made Easier by Partial Hydrogenation, Nano Lett 9(12) (2009) 4025-4030.
[58] A.F. Goncharov, Graphite at high pressures: Amorphization at 44 GPa, High Pressure Research 8(4) (1992) 607-616.
[59] A.F. Goncharov, I.N. Makarenko, S.M. Stishov, Graphite at pressures up to 55 GPa: Optical properties and raman spectra, High Pressure Research 4(1-6) (1990) 345-347.
[60] Y. Wang, M.G. Yao, Y.H. Chen, J.J. Dong, X.G. Yang, M.R. Du, R. Liu, H.B. Liu, Y.L. Li, B.B. Liu, Graphdiyne under pressure: A Raman study, Appl Phys Lett 113(2) (2018).
[61] M. Amsler, J.A. Flores-Livas, L. Lehtovaara, F. Balima, S.A. Ghasemi, D. Machon, S. Pailhes, A. Willand, D. Caliste, S. Botti, A. San Miguel, S. Goedecker, M.A.L. Marques, Crystal Structure of Cold Compressed Graphite, Phys Rev Lett 108(6) (2012).
[62] M. Hanfland, H. Beister, K. Syassen, Graphite under pressure: Equation of state and first-order Raman modes, Phys Rev B 39(17) (1989) 12598-12603.
[63] J. Schwan, S. Ulrich, V. Batori, H. Ehrhardt, S.R.P. Silva, Raman spectroscopy on amorphous carbon films, J Appl Phys 80(1) (1996) 440-447.